White pupae genes in the Tephritids *Ceratitis capitata, Bactrocera dorsalis* and *Zeugodacus cucurbitae*: a story of parallel mutations

Short title: **Genetic mutations causing white pupae phenotypes**

Ward CM[a,1], Aumann RA[b,1], Whitehead MA[c], Nikolouli K[d], Leveque G [e,f], Gouvi G[d,g], Fung E[h], Reiling SJ[e], Djambazian H[e], Hughes MA[c], Whiteford S[c], Caceres-Barrios C[d], Nguyen TNM[a,k], Choo A[a], Crisp P[a,h], Sim S[i], Geib S[i], Marec F[j], Häcker I[b], Ragoussis J[e], Darby AC[c], Bourtzis K[d,*], Baxter SW[k,*], Schetelig MF[b,*]

[a] School of Biological Sciences, University of Adelaide, Australia, 5005

[b] Justus-Liebig-University Gießen, Institute for Insect Biotechnology, Department of Insect Biotechnology in Plant Protection, Winchesterstr. 2, 35394 Gießen, Germany

[c] Centre for Genomic Research, Institute of Integrative Biology, The Biosciences Building, Crown Street, Liverpool, L69 7ZB, United Kingdom

[d] Insect Pest Control Laboratory, Joint FAO/IAEA Division of Nuclear Techniques in Food and Agriculture, Seibersdorf, A-1400 Vienna, Austria

[e] McGill University Genome Centre, McGill University, Montreal, Quebec, Canada

[f] Canadian Centre for Computational Genomics (C3G), McGill University, Montreal, Quebec, Canada

[g] Department of Environmental Engineering, University of Patras, 2 Seferi str., 30100 Agrinio, Greece

[h] South Australian Research and Development Institute, Waite Road, Urrbrae, South Australia 5064

[i] USDA-ARS Daniel K. Inouye US Pacific Basin Agricultural Research Center, 64 Nowelo Street, Hilo, Hawaii, 96720, USA

[j] Biology Centre, Czech Academy of Sciences, Institute of Entomology, Branišovská 31, 370 05 České Budějovice, Czech Republic

[k] Bio21 Molecular Science and Biotechnology Institute, School of BioSciences, University of Melbourne, Australia, 3010

1 Authors contributed equally to the study

* Corresponding authors:

k.bourtzis@iaea.org
simon.baxter@unimelb.edu.au
marc.schetelig@agrar.uni-giessen.de

Contributions

RA, CMW, CC, PC, SS, SG, IH, JR, ACD, KB, SWB, MFS designed research; CMW, RA, MAW, KN, GG, EF, SR, MAH, CC, TNMN, AC, SS, SG, ACD, KB, SWB, MFS performed research; RA, CMW, HD, GL, FM, JR, KB, SWB, MFS contributed new reagents/analytic tools; CMW, RA, MAW, KN, GL, GG, HD, SW, TNMN, AC, SS, SG, IH, JR, ACD, KB, SWB, MFS analyzed data; RA, CMW, KN, GL, GG, SR, SW, AC, SS, SG, IH, JR, ACD, KB, SWB, MFS wrote the paper.

Abstract (<250 words)

Flooding insect pest populations with huge numbers of sterilized males is an effective mean of biological control as they mate with, but cannot fertilize, wild females. The greatest challenge of the sterile insect technique (SIT) is the removal of unrequired factory reared females prior to sterilization and release. Spontaneous white-pupae (*wp*$^-$) color mutations have been integrated as a dimorphic selectable marker into historical SIT strains for three major tephritid fruit fly pests, *Bactrocera dorsalis*, *Ceratitis capitata* and *Zeugodacus cucurbitae*. Here we identify parallel genetic mutations causing the phenotype in all three species using diverse experimental approaches. The *B. dorsalis wp*$^-$ locus was introgressed into a related species, *Bactrocera tryoni,* and whole-genome sequencing identified a 37 bp truncating mutation within a gene containing a Major Facilitator Superfamily domain (MFS). In *C. capitata* and *Z. cucurbitae*, cytogenetics, comparative genomics and transcriptomic analysis of strains carrying brown and white pupae phenotypes identified an 8,150 bp insertion of a putative transposon into the *C. capitata* MFS ortholog and a 13 bp deletion in the *Z. cucurbitae* ortholog. In *B. tryoni* CRISPR/Cas9-mediated knock-out of the putative *Bt_wp* developed mosaic white and brown puparium colors in G_0, and G_1 progeny with recessive white pupae phenotypes. In *C. capitata,* complementation crosses of CRISPR-induced *wp*$^-$ mutants to flies carrying the naturally occurring recessive *wp*$^-$ mutation confirmed the role of the gene. Gene editing technology carries the potential for engineering white pupae phenotypes and generating dimorphic SIT strains in other tephritids or insect pest species.

Keywords (> 3 words)

introgression, chromosomal inversions, Sterile Insect Technique, genetic sexing strains, pest control, dimorphic markers

62 **Significance statement (<120 words)**

63 Mass releases of sterilized male insects within sterile insect technique programs have helped
64 suppress insect pest populations since the 1970s. In the major horticultural pests *Bactrocera*
65 *dorsalis, Ceratitis capitata,* and *Zeugodacus cucurbitae,* a key phenotype white pupae (wp)
66 has been used for decades to selectively remove females before releases, yet the gene
67 responsible remained unknown. Here we use classical and modern genetic approaches to
68 identify and functionally characterize causal *wp*$^-$ mutations in distantly related fruit fly species
69 and show it can be used to rapidly generate novel *wp*$^-$ strains. The conserved phenotype and
70 independent nature of the *wp*$^-$ mutations suggest that this technique can provide a generic
71 approach to produce sexing strains in other significant medical and agricultural insect pests.

72 **Introduction**

73 Tephritid species, including the Mediterranean fruit fly (medfly) *Ceratitis capitata*, the oriental
74 fruit fly *Bactrocera dorsalis*, the melon fly *Zeugodacus cucurbitae* and the Queensland fruit fly
75 *Bactrocera tryoni*, are major agricultural pests worldwide (1). The sterile insect technique (SIT)
76 is a species-specific and environment-friendly approach to control their populations, which has
77 been successfully applied as a component of area-wide integrated pest management
78 programs (2-4). The efficacy and cost-effectiveness of these large-scale operational SIT
79 applications has been significantly enhanced by the development and use of genetic sexing
80 strains (GSS) for Medfly, *B. dorsalis* and *Z. cucurbitae* (5, 6).

81 A GSS requires two principal components: a selectable marker, which could be phenotypic
82 or conditionally lethal, and the linkage of the wild type allele of this marker to the male sex,
83 ideally as close as possible to the male determining region. In a GSS, males are heterozygous
84 and phenotypically wild type, whilst females are homozygous for the mutant allele thus
85 facilitating sex separation (6-8). Pupal color was one of the first phenotypic traits exploited as
86 a selectable marker for the construction of GSS. In all three species, brown is the typical pupae
87 color. However, naturally occurring color mutants such as white pupae (*wp*) (9) and dark
88 pupae (*dp*) (10) have occurred in the field or laboratory stocks. The *wp* locus was successfully
89 used as a selectable marker to develop GSS for *C. capitata*, *B. dorsalis* and *Z. cucurbitae* (6,
90 11, 12), however, its genetic basis has never been resolved.

91 Biochemical studies provided evidence that the white pupae phenotype in medfly is due to
92 a defect in the mechanism responsible for the transfer of catecholamines from the hemolymph
93 to the puparial cuticle (13). In addition, classical genetic studies showed that the *wp* phenotype
94 is due to a recessive mutation in an autosomal gene located on chromosome 5 of the medfly
95 genome (9, 14). The development of translocation lines combined with deletion and
96 transposition mapping and advanced cytogenetic studies allowed the localization of the gene
97 responsible for the wp phenotype on the right arm of chromosome 5, at position 59B of the
98 trichogen polytene chromosome map (15). In the same series of experiments, the *wp* locus
99 was shown to be tightly linked to a *temperature-sensitive lethal (tsl)* gene (position 59B-61C),
100 which is the second selectable marker of the VIENNA 7 and VIENNA 8 GSS currently used in
101 all medfly SIT operational programs worldwide (7, 15).

102 The genetic stability of a GSS is a major challenge, mainly due to recombination
103 phenomena taking place between the selectable marker and the translocation breakpoint. To
104 address this risk, a chromosomal inversion called D53 was induced and integrated into the
105 medfly VIENNA 8 GSS (VIENNA 8^{D53+}) (6, 8). Cytogenetic analysis indicated that the D53
106 inversion spans a large region of chromosome 5 (50B-59C on trichogen polytene chromosome
107 map) with the *wp* locus being inside the inversion, close to its right breakpoint (6).

108 Extensive genetic and cytogenetic studies facilitated the development of a physical map of
109 the medfly genome (8, 16). The annotated gene set provided opportunities for the identification
110 of genes or loci-associated mutant phenotypes, such as the *wp* and *tsl*, used for the
111 construction of GSS (16, 17). Salivary gland polytene chromosome maps developed for *C.*
112 *capitata*, *B. dorsalis*, *Z. cucurbitae,* and *B. tryoni* show that their homologous chromosomes
113 exhibit similar banding patterns. In addition, *in situ* hybridization analysis of several genes
114 confirmed that there is extensive shared synteny, including the right arm of chromosome 5
115 where the *C. capitata wp* gene is localized (8). Interestingly, two recent studies identified SNPs
116 associated with the *wp* phenotype in *C. capitata* and *Z. cucurbitae* that were also on
117 chromosome 5 (18, 19).
118 In the present study, we employed different strategies involving genetics, cytogenetics,
119 genomics, transcriptomics, gene editing and bioinformatics to identify independent natural
120 mutations in a novel gene responsible for pupal coloration in three tephritid species of major
121 agricultural importance, *C. capitata*, *B. dorsalis*, and *Z. cucurbitae*. We then functionally
122 characterized causal mutations within this gene in *C. capitata* and *B. tryoni* resulting in
123 development of new white pupae strains. Due to its conserved nature (20) and widespread
124 occurrence in many insect species of agricultural and medical importance, we also discuss
125 the potential use of this gene as a generic selectable marker for the construction of GSS for
126 SIT applications.

Results

Resolving the *B. dorsalis wp* locus with interspecific introgression. The *B. dorsalis white pupae* phenotype was introgressed into *B. tryoni* to generate a strain referred to as the *Bactrocera Introgressed Line* (*BIL,* Fig. S1). To determine the proportion of *B. dorsalis* genome introgressed into *BIL*, whole genome sequence data from male and female *B. dorsalis*, *B. tryoni,* and *BIL* individuals were analyzed. Paired end Illumina short read data from single *B. oleae* males (SRR826808) and females (SRR826807) were used as an outgroup. Single copy orthologs across the genome (n = 1,846) were used to reconstruct the species topology revealing species-specific monophyly (Fig. 1A) consistent with previously published phylogenies (21, 22). Reconstruction also showed monophyly between *B. tryoni* and *BIL* across 99.2% of gene trees suggesting the majority of loci originally introgressed from *B. dorsalis* have been removed during backcrosses.

Genomes were partitioned into 100 kb windows and pairwise absolute genetic distance (d_{XY}) calculated between each species and *BIL* to estimate admixture. *B. dorsalis* was found to be highly similar to a small proportion of the *BIL* genome (Fig. 1B; purple), as indicated by d_{XY} values approaching the median value of *B. dorsalis* vs *B. tryoni* (Fig. 1B; orange).

Two formal tests for introgression were also carried out, the f estimator $\widehat{f_d}$ (Fig. 1C) and topology weighting (Fig. 1D). Three distinct local evolutionary histories (Fig. 1D) were tested using d_{XY} and topology weighting across the *B. dorsalis wp* Quantitative Trait Locus (QTL) i) *BIL* is closest to *B. tryoni* (Fig. 1D; purple, expected across most of the genome), ii) *BIL* is closest to *B. dorsalis* (Fig. 1D; orange, expected at the wp^- locus), and iii) *BIL* is closest to *B. oleae* (Fig. 1D; green, a negative control). Across the nuclear genome the species topology was supported in 98.82% of windows. Both $\widehat{f_d}$ and topology weighting confirmed a lack of widespread introgression from *B. dorsalis* into *BIL* with few (n = 42) discordant outlier windows. Genomic windows discordant across all three tests were considered candidate regions for the *wp* mutation. Four scaffolds accounting for 1.18% of the *B. dorsalis* genome met these criteria and only two, NW_011876372.1 and NW_011876398.1, showed homozygous introgression consistent with a recessive white pupae phenotype (Fig. S2).

To resolve breakpoints within the *B. dorsalis wp* QTL, a 10 kb windowed analysis across NW_011876398.1 and NW_011876372.1 was performed using d_{XY} (Fig. 1E), topology weighting (Fig. 1F) and $\widehat{f_d}$ (Fig. 1G). The maximum range of the introgressed locus was 4.49 Mbp (NW_011876398.1 was 2.9-5.94 Mb and NW_011876372.1 was 0-1.55 Mb) (Fig. 1E-G). The wp^- QTL was further reduced to a 2.71 Mb region containing 113 annotated protein coding genes through analyzing nucleotide diversity (π) among eight pooled BIL genomes (3.8 Mb on NW_011876398.1 to 0.73 Mb on scaffold NW_011876372.1, Fig. S2).

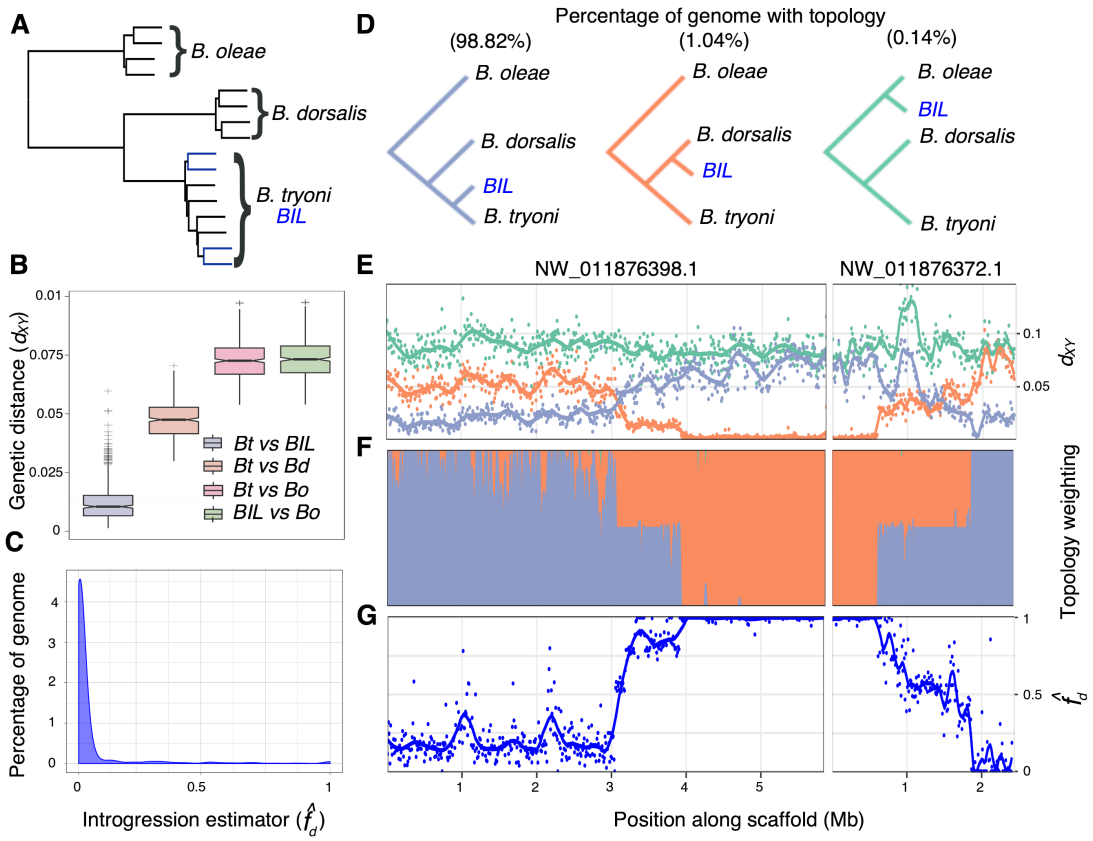

Fig. 1. Characterization of total introgression from *B. dorsalis* into the *Bactrocera Introgressed Line* and identification of the *white pupae* locus. (A) Species tree constructed from 1,846 single copy ortholog gene trees for four haplotypes of *B. oleae, B. dorsalis, B. tryoni* and *BIL*. Branches corresponding to *BIL* individuals are shown in blue. All nodes were well supported with posterior probabilities >0.97. (B) Nei's absolute genetic distance (d_{XY}) calculated for tiled 100 kb windows across the genome between *B. tryoni* vs *BIL (*Bt vs BIL*); B. tryoni* vs *B. dorsalis* (*Bt* vs *Bd*); *B. tryoni* vs *B. oleae* (*Bt* vs *Bo*) and *BIL* vs *B. oleae* (*BIL* vs *Bo*). (C) The introgression estimator ($\hat{f}_d$) calculated across tiled 100 kb windows to identify regions of disproportionately shared alleles between *BIL* and *B. dorsalis*, $\hat{f}_d$ (*Bt*, *BIL*, *Bd*; *Bo*). (D) The three evolutionary hypothesis/topologies of interest to identify introgressed regions and their representation across the genome: species (purple, 98.82%), introgression (orange, 1.04%) and a negative control tree (green, 0.14%). (E) Nei's absolute genetic distance (d_{XY}) calculated for tiled 10 kb windows across the candidate *wp* locus colors follow the legend in (D). (F) Topology weighting for each topology shown in (D) calculated for 1 kb tiled local trees across the candidate *wp* locus. (G) The introgression estimator ($\hat{f}_d$) calculated across tiled 10 kb windows, $\hat{f}_d$ (*Bt*, *BIL*, *Bd*; *Bo*).

Resolving the *C. capitata* D53 inversion breakpoints and *wp* locus with genome sequencing and *in situ* hybridization. Previous cytogenetic studies determined the localization of the gene responsible for the white pupae phenotype on the right arm of chromosome 5, at position 59B of the trichogen polytene chromosome map (15). The equivalent of position 59B is position 76B of the salivary gland polytene chromosome map, inside but close to the right breakpoint of the D53 inversion (69C-76B on the salivary gland polytene chromosome map). Long read sequencing data were generated of the wild type strain Egypt II (EgII), the inversion line D53 and the genetic sexing strain VIENNA 8 (without

186 the inversion; VIENNA $8^{D53-|-}$) (Table S1) to enable a comparison of the genomes and locate
187 the breakpoints of the D53 inversion, to subsequently narrow down the target region, and to
188 identify *wp* candidate genes.
189 Chromosome 5-specific markers (16) were used to identify the EgII_Ccap3.2.1 scaffold_5
190 as complete chromosome 5. Candidate D53 breakpoints in EgII scaffold_5 were identified
191 using the alignment of three genome datasets EgII, VIENNA $8^{D53-|-}$, and D53 (see methods).
192 The position of the D53 inversion breakpoints was located between 25,455,334 – 25,455,433
193 within a scaffold gap (left breakpoint), and at 61,880,224 bp in a scaffolded contig (right
194 breakpoint) on EgII chromosome 5 (Ccap3.2.1; accession GCA_902851445). The region
195 containing the causal *wp* gene was known to be just next to the right breakpoint. Cytogenetic
196 analysis and *in situ* hybridization using the wild type EgII strain and the D53 inversion line
197 confirmed the overall structure of the inversion, covering the area of 69C-76B on the salivary
198 gland polytene chromosomes (Fig. 2), as well as the relative position of markers residing
199 inside and outside the breakpoints (Fig. 2 and Fig. S3). PCRs using two primer pairs flanking
200 the predicted breakpoints (Fig. S4C) and subsequent sequencing confirmed the exact
201 sequence of the breakpoints. Using a primer combination specific for the chromosome 5 wild
202 type status confirmed in the WT in EgII flies and VIENNA $7^{D53+|-}$ GSS males, which are
203 heterozygous for the inversion. Correspondingly, these amplicons were not present in D53
204 males and females or in VIENNA $7^{D53+|+}$ GSS females (all homozygous for the inversion) (Fig.
205 S4A-B). Positive signals for the inversion were detected in D53 and VIENNA 7^{D53+} GSS males
206 and females, but not in WT flies using an inversion-specific primer pair (Fig. S4D-E).

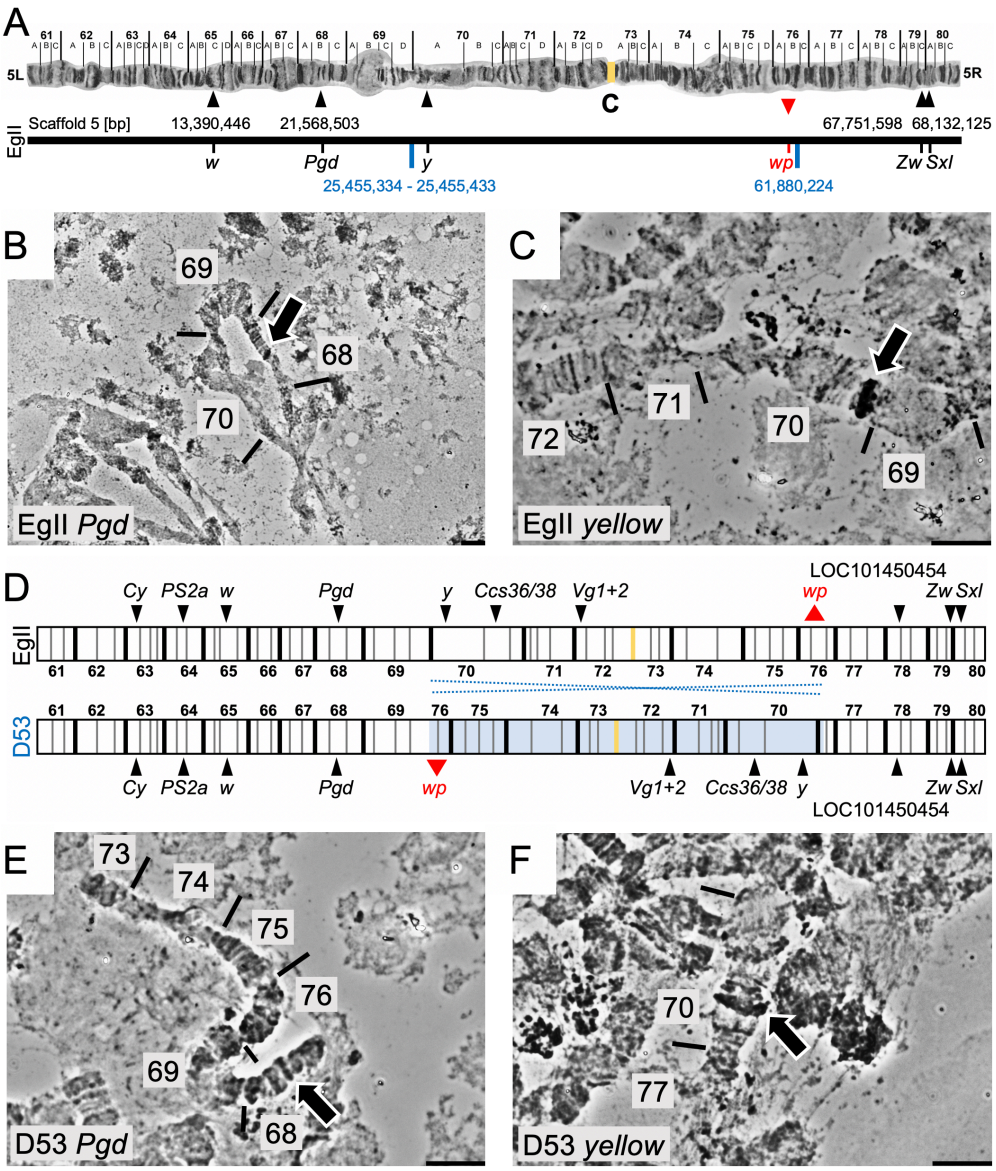

Fig. 2. Genomic positioning of the D53 inversion on chromosome 5 of *C. capitata*. (A) Chromosome scale assembly of *C. capitata* EgII chromosome 5. Shown are the positions of *in situ* mapped genes *white* (*w*), *6-phosphogluconate dehydrogenase* (*Pgd*), *glucose-6-phosphate 1-dehydrogenase* (*Zw*) and *sex lethal* (*Sxl*), the position of the D53 inversion breakpoints (blue), and the relative position of *white pupae* (*wp*) on the polytene chromosome map of chromosome 5 (23) and the PacBio-Hi-C EgII scaffold_5, representing the complete chromosome 5 (genome Ccap3.2.1, accession GCA_902851445). The position of the *yellow* gene (*y*, LOC101455502) was confirmed on chromosome 5 70A by *in situ* hybridization, despite its sequence not been included in the scaffold assembly. (D) Schematic illustration of chromosome 5 without (EgII, WT) and with (D53) D53 inversion. The inverted part of chromosome 5 is shown in light blue. Two probes, one inside (*y,* 70A) and one outside (*Pgd*, 68B) of the left inversion breakpoint were used to verify the D53 inversion breakpoints by *in situ* hybridization. WT EgII is shown in (B) and (C), D53 in (E) and (F).

221 **Genome and transcriptome sequencing lead to a single candidate *wp*$^{-}$ gene in *B.***
222 ***dorsalis, C. capitata, and Z. cucurbitae***.
223 Orthologs within the QTL of *B. dorsalis, C. capitata* and scaffolds previously identified to
224 segregate with the *wp*$^{-}$ phenotype in *Z. cucurbitae* (NW_011863770.1 and NW_011863674.1
225 (18)) were investigated for high effect mutations under the assumption that a null mutation in
226 a conserved gene results in the *wp*$^{-}$ phenotype. A single ortholog contained fixed indels absent
227 from wild type strains was identified in each species*. White pupae B. dorsalis* and *BIL* strains
228 showed a 37 bp frame-shift deletion in the first coding exon of LOC105232189 introducing a
229 premature stop codon 210 bp from the transcription start site (Fig. 3). Presence of the deletion
230 was confirmed *in silico* using whole genome resequencing from the *wp* and wildtype mapped
231 to the reference, and by *de novo* assembly of Illumina RNAseq data transcripts (Fig. 3).
232 In *C. capitata*, *wp* individuals D53 Nanopore read alignment on EgII showed an
233 independent approximate 8,150 bp insertion into the third exon of LOC101451947 disrupting
234 proper gene transcription 822 bp from the transcription start site (Fig. 3). The insertion
235 sequence is flanked by identical repeats, suggesting that it may originate from a transposable
236 element insertion. The *C. capitata* mutation was confirmed *in silico,* as in *B. dorsalis,* using
237 whole genome sequencing and RNAseq data (Fig. 3).
238 Transcriptome data from the white pupae-based genetic sexing strain of *Z. cucurbitae*
239 revealed a 13 bp deletion in the third exon of LOC105216239 on scaffold NW_011863770.1
240 introducing a premature stop codon (Fig. 3).
241 The candidate *white pupae* gene in all three species had a reciprocal best BLAST hit to the
242 putative metabolite transport protein CG14439 in *Drosophila melanogaster* and contains a
243 Major Facilitator-like superfamily domain (MFS_1, pfam07690), suggesting a general function
244 as a metabolite transport protein. *In situ* hybridization on polytene chromosomes of *B. dorsalis*,
245 *C. capitata* and *Z. cucurbitae* was used to confirm the presence of the *wp* locus in the same
246 syntenic position on the right arm of chromosome 5 (Fig. 3). Therefore, all three species show
247 a mutation in the same positional orthologous gene likely to be responsible for the phenotype
248 in all three genera.

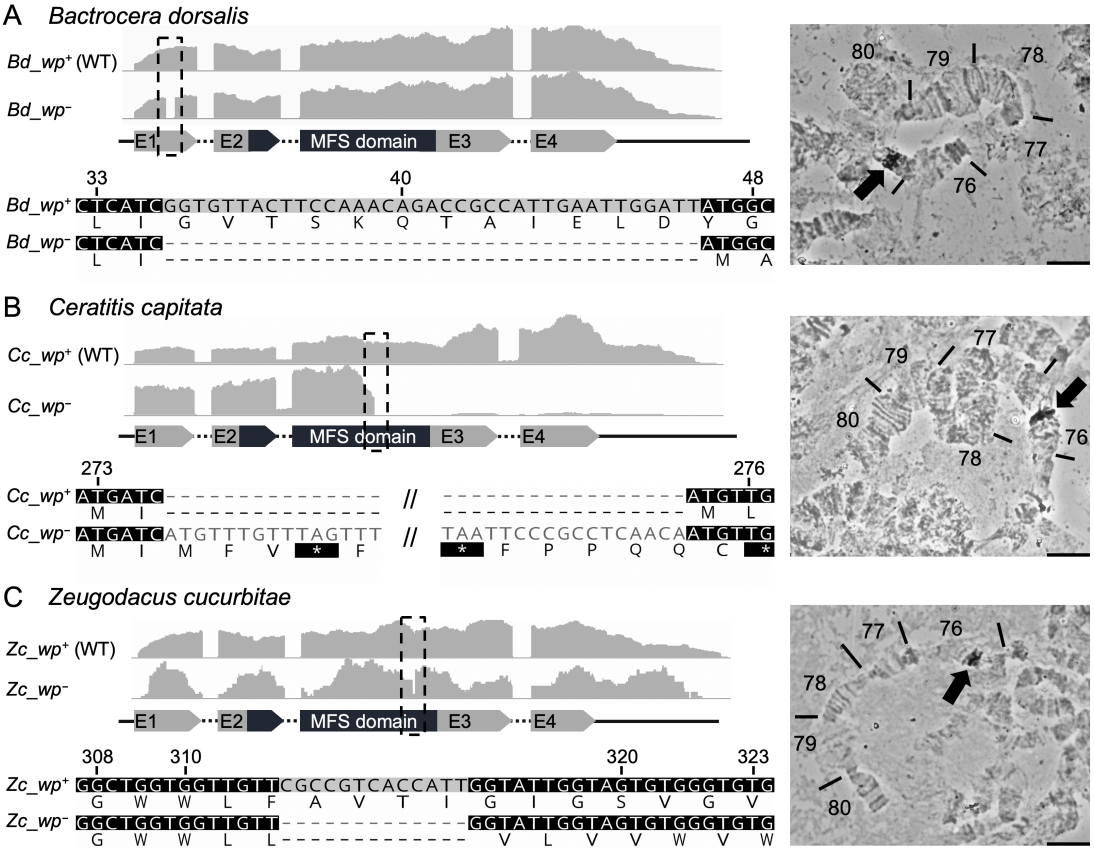

Fig. 3. Identification of the *wp* mutation in the transcriptomes of *B. dorsalis*, *C. capitata* and *Z. cucurbitae*. The grey graphs show expression profiles from the candidate *wp* loci in WT (wp^+) and mutant (wp^-) flies at the immobile pupae stages of (A) *B. dorsalis*, (B) *C. capitata* and (C) *Z. cucurbitae*. The gene structure (not drawn to scale) is indicated below as exons (arrows labelled E1-E4) and introns (dashed lines). The positions of independent *wp* mutations (*Bd*: 37 bp deletion, *Cc*: approximate 8,150 bp insertion, *Zc*: 13 bp deletion) are marked with black boxes in the expression profiles and are shown in detail below the gene models based on *de novo* assembly of RNAseq data from WT and white pupae phenotype individuals. *In situ* hybridization on polytene chromosomes (right) confirmed the presence of the *wp* locus on the right arm of chromosome 5 in all three species (arrows in micrographs).

CRISPR/Cas9 knockout of a Major Facilitator Superfamily gene in *B. tryoni* and *C. capitata* causes the white pupae phenotype. An analogous *B. dorsalis* wp^- mutation was developed in *B. tryoni* by functional knockouts of the putative *Bt_wp* using the CRISPR/Cas9 system. A total of 591 embryos from the Ourimbah laboratory strain were injected using two guides with recognition sites in the first coding exon of this gene (Fig. 4A). Injected embryos surviving to adulthood (n = 19, 3.2%) developed with either wild type brown (n=12) or somatically mosaic white-brown puparia (n = 7, Fig. S5). Surviving G_0 adults were individually backcrossed into the Ourimbah strain, resulting in potentially $wp^{+|-(CRISPR)}$ heterozygous brown pupae (Fig. 4C). Five independent G_0 crosses were fertile (three mosaic white-brown and two brown pupae phenotypes), G_1 offspring were sibling mated and visual inspection of G_2

271 progeny revealed that three families contained *white pupae* individuals. Four distinct
272 frameshift mutations were observed in screened G_2 progeny (Fig. 4A) suggesting functional
273 KO of putative *Bt_wp* is sufficient to produce the *white pupae* phenotype in *B. tryoni*. Capillary
274 sequencing of cloned *Bt_MFS* amplicons revealed deletions ranging from a total of 4 bp to
275 155 bp, summed across the two guide recognition sites, introducing premature stop codons.
276 In *C. capitata,* CRISPR/Cas9 gene editing was used to knock-out the orthologous gene and
277 putative *Cc_wp*, LOC101451947, to confirm that it causes a wp^- phenotype. A mix of
278 recombinant Cas9 protein and the gRNA_MFS, targeting the third exon and thereby the MFS
279 domain of the presumed *Cc_wp* CDS (Fig. 4B), was injected into 588 EgII WT embryos of
280 which 96 developed to larvae and 67 pupated. All injected G_0 pupae showed brown pupal
281 color. In total, 29 G_0 males and 34 females survived to adulthood (9.3%) and were
282 backcrossed individually or in groups (see material and methods) to a strain carrying the
283 naturally occurring white pupae mutation ($wp^{-(nat)}$; strain #1402_22m1B) (24) (Fig. 4D). As
284 w*hite pupae* is known to be monogenic and recessive in *C. capitata*, this complementation
285 assay was used to reveal whether the targeted gene is responsible for the naturally occurring
286 white pupae phenotype or if the mutation is located in a different gene. G_1 offspring would only
287 show white pupae phenotypes if *Cc_wp* was indeed the *white pupae* gene, knocked-out by
288 the CRISPR approach, and complemented by the natural mutation through the backcross ($wp^{-(nat)|-(CRISPR)}$).
289 In the case that the *Cc_wp* is not the gene carrying the natural wp^- mutation, a
290 brown phenotype would be observed for all offspring. Here, five out of 13 crosses, namely M1,
291 M3, F2, F3, and F4, produced white pupae phenotype offspring. The crosses generated 221,
292 159, 70, 40, and 52 G_1 pupae, of which 10, 30, 16, 1, and 1 pupa respectively, were white.
293 Fifty-seven flies emerged from white pupae were analyzed via non-lethal genotyping, and all
294 of them showed mutation events within the target region. Overall, eight different mutation
295 events were seen, including deletions ranging from 1-9 bp and a 46 bp deletion combined with
296 a 2 bp insertion (Fig. 4B). Five mutation events (B, D, E, G, H) caused frameshifts and
297 premature stop codons. The remaining three (A, C, F), however, produced deletions of only
298 one to three amino acids. To make $wp^{-(CRISPR)}$ mutations homozygous, mutants were either
299 inbred (mutation C) (Fig. 4D) or outcrossed to WT EgII (mutation A-H), both in groups
300 according to their genotype. This demonstrated that *Cc_wp* is the gene carrying the $wp^{-(nat)}$,
301 and that even the loss of a single amino acid without a frameshift at this position can cause
302 the white pupae phenotype. Offspring from outcrosses of mutation A, D, and H, as well as
303 offspring of the inbreeding (mutation C), were genotyped via PCR, and $wp^{+|-(CRISPR)}$ and $wp^{-(CRISPR)|-(CRISPR)}$
304 positive flies were inbred to establish pure new *white pupae* lines.

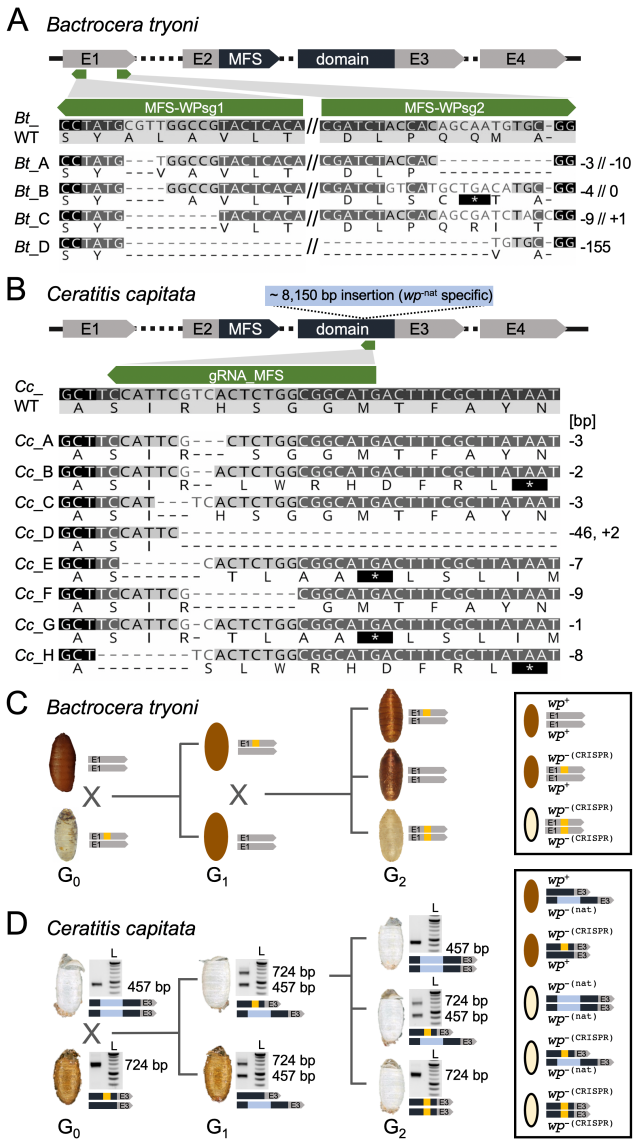

Fig. 4. CRISPR/Cas9-based generation of homozygous *wp*$^{-(CRISPR)}$ lines in *B. tryoni* and *C. capitata*. A schematic structure of the *wp* CDS exons (E1, E2, E3, E4) including the MFS domain in *B. tryoni* (A) and *C. capitata* (B) are shown. Positions of gRNAs targeting the first and third exon in *B. tryoni* and *C. capitata,* respectively, are indicated by green arrows. Nucleotide and amino acid sequences of mutant *wp* alleles identified in G_1 individuals are compared to the WT reference sequence in *B. tryoni* (A) and *C. capitata* (B). Deletions are shown as dashes, alterations on protein level leading to premature stop codons are depicted as asterisks highlighted in black. Numbers on the right side represent InDel sizes (bp = base pairs). Crossing schemes to generate homozygous *wp*$^{-(CRISPR)}$ lines in *B. tryoni* (C) and *C. capitata* (D) show different strategies to generate *wp* strains. Bright field images of empty puparia are depicted for both species. Genotype schematics and corresponding PCR analysis (for *C. capitata*) validating the presence CRISPR-induced (orange) and natural (blue, for *C. capitata*) *wp* mutations are shown next to the images of the puparia. (C) Injected G_0 *B. tryoni* were backcrossed to the Ourimbah laboratory strain resulting in uniformly brown G_1 offspring (depicted as illustration because no images were acquired during G_1). G_1 inbreeding led to G_2 individuals homozygous for the white pupae phenotype. (D) Injected WT G_0 flies were crossed to flies homozygous for the naturally occurring *wp*$^-$ allele (*wp*$^{-(nat)}$). *wp*$^{-(nat)}$ (457 bp amplicon) and *wp*$^{-(CRISPR)}$ or WT (724 bp amplicon) alleles were identified by multiplex PCR (left lane; L = NEB 2log ladder). White pupae phenotypes in G_1 indicated positive CRISPR events. G_2 flies with a white pupae phenotype that were homozygous for *wp*$^{-(CRISPR)}$ allele were used to establish lines.

Discussion

White pupae (*wp*) was first identified in *C. capitata* as a spontaneous mutation and was subsequently adopted as a phenotypic marker of fundamental importance for the construction of GSS for SIT (6, 9). Full penetrance expressivity and recessive inheritance rendered *wp* the marker of choice for GSS construction in two additional tephritid species, *B. dorsalis* and *Z. cucurbitae* (11, 12), allowing automated sex sorting based on pupal color. This was only possible because spontaneous *wp* mutations occur at relatively high rates either in the field or in mass rearing facilities and can easily be detected (6, 9). Despite the easy detection and establishment of *wp* mutants in these three species, similar mutations have not been detected in other closely or distantly related species such as *B. tryoni*, *B. oleae,* or *Anastrepha ludens* despite large screens being conducted. In addition to being a visible GSS marker used to separate males and females, the *wp* phenotype is also important for detecting and removing recombinants in cases where sex separation is based on a conditional lethal gene such as the *tsl* gene in the medfly VIENNA 7 or VIENNA 8 GSS (6, 7). However, it took more than 20 years from the discovery and establishment of the *wp* mutants to the large-scale operational use of the medfly VIENNA 8 GSS for SIT applications (6, 9) and the genetic nature of the *wp* mutation remained unknown. The discovery of the underlying *wp* mutations and the availability of CRISPR/Cas genome editing would allow the fast recreation of such phenotypes and sexing strains in other insect pests. Isolation of the *wp* gene would also facilitate future efforts towards the identification of the closely linked *tsl* gene.

Using an integrated approach consisting of genetics, cytogenetics, genomics, transcriptomics and bioinformatics, we identified the white pupae (*wp*) genetic locus in three major tephritid agricultural pest species, *B. dorsalis*, *C. capitata,* and *Z. cucurbitae*.

Our study clearly shows the power of employing different strategies for gene discovery, one of which was species hybridization. In *Drosophila*, hybridization of different species has played a catalytic role in the deep understanding of species boundaries and the speciation processes, including the evolution of mating behavior and gene regulation (25-29). In our study, we took advantage of two closely related species, *B. dorsalis* and *B. tryoni*, which can produce fertile hybrids and be backcrossed for consecutive generations. This allowed the introgression of the *wp* mutant locus of *B. dorsalis* into *B. tryoni,* resulting in the identification of the introgressed region, including the causal *wp* mutation via whole-genome resequencing and advanced bioinformatic analysis.

In *C. capitata*, we exploited two essential pieces of evidence originating from previous genetic and cytogenetic studies: the localization of wp to region 59B and 76B on chromosome 5 in the trichogen cells and salivary gland polytene chromosome map, respectively (15, 30), and its position close to the right breakpoint of the large inversion D53 (6). This data prompted

362 us to undertake a comparative genomic approach to identify the exact position of the right
363 breakpoint of the D53 inversion, which would bring us in the vicinity of the *wp* gene. Coupled
364 with comparative transcriptomic analysis, this strategy ensured that the analysis indeed
365 tracked the specific *wp* locus on the right arm of chromosome 5, instead of any mutation in
366 another, random locus which may participate in the pigmentation pathway and therefore result
367 in the same phenotype. Functional characterization via CRISPR/Cas9-mediated knock-out
368 resulted in the establishment of new white pupae strains in *C. capitata* and *B. tryoni* and
369 confirmed that this gene is responsible for the pupal coloration in these tephritid species.
370 Interestingly, the wp phenotype is based on three independent and very different natural
371 mutations of this gene, a rather large and transposon-like insertion in *C. capitata*, but only
372 small deletions in the two other tephritids, *B. dorsalis* and *Z. cucurbitae*. Also in medlfy,
373 however, CRSIRP-induced in-frame deletions of one or three amino acids in the MFS domain
374 were sufficient to induce the wp phenotype, underlining the importance of this domain for
375 correct pupal coloration.

376 It is worth noting, that in the first stages of this study, we employed two additional
377 approaches, which did not allow us to successfully narrow down the *wp* genomic region to the
378 desired level. The first was based on Illumina sequencing of libraries produced from laser
379 micro-dissected (Y;5) mitotic chromosomes that carry the wild type allele of the *wp* gene
380 through a translocation from the fifth chromosome to the Y. This dataset from the medfly
381 VIENNA 7 GSS was comparatively analyzed to wild type (Egypt II) Y and X chromosomes,
382 and the complete genomes of Egypt II, VIENNA 7 $^{D53-}$ GSS, and a D53 inversion line in an
383 attempt to identify the chromosomal breakpoints of the translocation and/or inversion, which
384 are close to the *wp* locus (Table S2). However, this effort was not successful due to the short
385 Illumina reads and the lack of a high-quality reference genome. The second approach was
386 based on individual scale whole-genome resequencing/genotyping, and identifying fixed loci
387 associated with pupal color phenotypes, which complemented the QTL analysis (19). Seven
388 loci associated with SNPs and larger deletions linked to the white pupae phenotype were
389 analyzed based on their respective mutations and literature searches for their potential
390 involvement in pigmentation pathways. However, we could not identify a clear link to the pupal
391 coloration as shown by *in silico*, molecular, and *in situ* hybridization analysis (Supplementary
392 text S1, Fig. S6 and S7, Table S3).

393 The *wp* gene is a member of a major facilitator superfamily (MFS). Orthologs of *white pupae*
394 are present in 146 of 148 insect species aggregated in OrthoDB v9 (20) present in all orders
395 and single copy in 133 species. Furthermore, wp is included in the benchmarking universal
396 single copy ortholog (BUSCO) gene set for insecta and according to OrthoDB v10 (31) has a
397 below average evolutionary rate (0.87, OrthoDB group 42284at50557) suggesting an
398 important and evolutionarily conserved function (Fig. S8). Its ortholog in *Bombyx mori*, *mucK*,

399 was shown to participate in the pigmentation at the larval stage (32) whereas in *D.*
400 *melanogaster* peak expression is during the prepupal stage after the larva has committed to
401 pupation (33), which is the stage where pupal cuticle sclerotization and melanization occurs.
402 It is known that the insect cuticle consists of chitin, proteins, lipids and catecholamines, which
403 act as cross-linking agents thus contributing to polymerization and the formation of the
404 integument (34). Interestingly, the sclerotization and melanization pathways are connected
405 and this explains the different mechanical properties observed in different medfly pupal color
406 strains with the "dark" color cuticles to be harder than the "brown" ones and the latter harder
407 than the "white" color ones (35). The fact that the white pupae mutants are unable to transfer
408 catecholamines from the haemolymph to the cuticle is perhaps an explanation for the lack of
409 the brown pigmentation (13).

410 The discovery of the long-sought *wp* gene in this study and the recent discovery of the
411 *Maleness-on-the-Y* (*MoY*) gene, which determines the male sex in several tephritids (36),
412 opens the way for the development of a 'generic approach' for the construction of GSS for
413 other species. Using CRISPR/Cas-based genome editing approaches, we can: (a) induce
414 mutations in the *wp* orthologues of SIT target species and establish lines with *wp* phenotype
415 and (b) link the rescue alleles as closely as possible to the *MoY* region. Given that the *wp*
416 gene is present in diverse insect species including agricultural insect pests and mosquito
417 disease vectors, this approach would allow more rapid development of GSS in SIT target
418 species. In principle, these GSS will have higher fertility compared to the semi-sterile
419 translocation lines (6). In addition, these new generation GSS will be more stable since the
420 rescue allele will be tightly linked to the male determining region thus eliminating
421 recombination which can jeopardize the genetic integrity of any GSS. The concept of the
422 'generic approach' can also be applied in species which lack a typical Y chromosome such as
423 *Aedes aegypti* and *Aedes albopictus*. In these species, the rescue allele should be transferred
424 close to the male determining gene (*Nix*) and the M locus (37, 38). It is hence important for
425 this 'generic approach' to identify regions close enough to the male determining loci to ensure
426 the genetic stability of the GSS and to allow the proper expression of the rescue alleles. In the
427 present study, we have already shown that CRISPR/Cas9-induced mutations resulting in the
428 white pupae phenotype can be developed in SIT target species and the resulting strains
429 provide already new opportunities for GSS based on visible markers.

430 **Material and methods**

431 All sequence libraries prepared during this study are publicly available on NCBI within the ENA
432 BioProject PRJEB36344/ERP119522 (accession numbers ERS4426857 - ERS4426873,
433 ERS4426994 - ERS4427029, ERS4519515; see table S1) and the BioProject PRJNA629430
434 (SRA accessions SRR11649127 - SRR11649132; see Supplementary text 1).
435
436 **Insect rearing.** *C. capitata*, *B. dorsalis* and *Z. cucurbitae* fly strains were maintained at
437 25±1°C, 48% RH and 14/10 h light/dark cycle. They were fed with a mixture of sugar and yeast
438 extract (3v:1v) and water. Larvae were reared on a gel diet, containing carrot powder (120 g/l),
439 agar (3 g/l), yeast extract (42 g/l), benzoic acid (4 g/l), HCl (25%, 5.75 ml/l) and ethyl-4-
440 hydroxybenzoate (2.86 g/l). Flies were anesthetized with N_2 or CO_2 for screening, sexing, and
441 the setup of crosses. To slow down the development during the non-lethal genotyping process
442 (*C. capitata*), adult flies were kept at 19°C, 60% RH, and 24 h light for this period (1-4 d).
443 *B. tryoni* flies were obtained from New South Wales Department of Primary Industries
444 (NSW DPI), Ourimbah, Australia and reared at 25 ± 2°C, 65 ± 10% RH and 14/10 h light/dark
445 cycle. Flies were fed with sugar, Brewer's yeast and water and larvae were reared on a gel
446 diet, containing Brewer's yeast (204 g/l), sugar (121 g/l), methyl p-hydroxy benzoate (2 g/l),
447 citric acid (23 g/l), wheat germ oil (2 g/l), sodium benzoate (2 g/l) and agar (10 g/l).
448
449 **Introgression and bioinformatic identification of a natural *wp* mutation from *B. dorsalis***
450 **in *B. tryoni.*** Interspecific crosses between *B. tryoni* and *white pupae B. dorsalis* were carried
451 out between male *B. tryoni* ($wp^{+|+}$) and female *B. dorsalis* ($wp^{-|-}$). The G_1 $wp^{+|-}$ hybrids
452 developed with brown puparia and were mass crossed. G_2 $wp^{-|-}$ females were backcrossed
453 into *B. tryoni* $wp^{+|+}$ males and backcrossing was then repeated for five additional times to
454 produce the *white pupae Bactrocera Introgressed Line* (BIL, Fig. S1).
455 Genome sequencing using Illumina NovaSeq (2 x 150 bp, Deakin University) was
456 performed on a single male and female from the *B. dorsalis wp* strain, *B. tryoni*, and the *BIL*
457 (~ 26X) and two pools of five *BIL* individuals (~32X). Quality control of each sequenced library
458 was carried out using FastQC v0.11.6
459 (https://www.bioinformatics.babraham.ac.uk/projects/fastqc/) and aggregated using
460 ngsReports v1.3 (39). Adapter trimming was carried out using Trimmomatic v0.38
461 (https://academic.oup.com/bioinformatics/article/30/15/2114/2390096) and paired reads were
462 mapped to the *B. dorsalis* reference genome (GCF_000789215.1) using NextGenMap v0.5.5
463 (40) under default settings. Mapped data were sorted and indexed using SAMtools, and
464 deduplication was carried out using Picard MarkDuplicates v2.2.4
465 (https://github.com/broadinstitute/picard). Genotypes were called on single and pooled

466 libraries separately with ploidy set to two and ten respectively using Freebayes v1.0.2 (41).
467 Each strain was set as a different population in Freebayes. Genotypes with less than five
468 genotype depth were set to missing and sites with greater than 20% missing genotypes or
469 indels filtered out using BCFtools v1.9 (42). Conversion to the genomic data structure (GDS)
470 format was carried out using SeqArray v1.26.2 (43) and imported into the R package geaR
471 v0.1 (https://github.com/CMWbio/geaR) for population genetic analysis.
472 Single copy orthologs were identified in the *B. dorsalis* reference annotated proteins (NCBI
473 *Bactrocera dorsalis* Annotation Release 100) with BUSCO v3 (44, 45) using the dipteran gene
474 set (44). Nucleotide alignments of each complete single copy ortholog were extracted from
475 the called genotype set using geaR v0.1 and gene trees built using RAxML v8.2.10 (46) with
476 a GTR+G model. Gene trees were then imported into Astral III v5.1.1 (47) for species tree
477 estimation. Genome scans of absolute genetic divergence (d_{XY}), nucleotide diversity (π), and
478 the f estimator $\widehat{f_d}$ were carried out using geaR v0.1. Two levels of analysis were carried out:
479 i) genome wide scans of non-overlapping 100 kb windows and ii) locus scans of 10 kb tiled
480 windows. Local phylogenies were built for nucleotide alignments of non-overlapping 1 kb
481 windows using RAxML v8.2.10 with a GTR+G model and topology weighting was calculated
482 using TWISST (48).
483 Introgressed regions (i.e. candidate *wp* loci) were identified by extracting windows in the
484 genome wide scan with topology weighting and fd greater than 0.75 and visually inspecting
485 the 'locus scan' data set for d_{XY}, fd and topology weighting patterns indicative of introgression.
486 Nucleotide alignments of all genes within candidate *B. dorsalis* introgressed regions were
487 extracted from the GDS using geaR and visually inspected for fixed mutations in *B. dorsalis*
488 *wp*, BIL individuals and the two BIL pools. Candidate genes were then searched by tBLASTn
489 against the *D. melanogaster* annotated protein set to identify putative functions and functional
490 domains were annotated using HMMer (49). Mapped read depth was calculated around
491 candidate regions using SAMtools depth v1.9 (50) and each sample's read depth was
492 normalized to the sample maximum to inspect putative deletions. Called genotypes were
493 confirmed by *de novo* genome assembly of the *B. dorsalis wp* genome using MaSuRCA v3.3
494 (51) under default settings. The *de novo* scaffold containing LOC105232189 was identified
495 using the BLASTn algorithm. *In silico* exon-intron boundaries were then manually annotated
496 in Geneious v11 (52).
497
498 **Identification, characterization and molecular analysis of the D53 inversion and *wp***
499 **locus in *C. capitata*.**
500 *Characteristics of* C. capitata *strains used for this study*
501 Egypt II (EgII) is a wild type laboratory strain. D53 is a homozygous strain with an irradiation-
502 induced inversion covering the area 69C-76B on the salivary gland polytene chromosome map

503 (50B-59C on the trichogen cells polytene chromosome map). VIENNA 7 and VIENNA 8 are
504 two GSS in which two (Y;5) translocations, on the region 58B and 52B of the trichogen cells
505 polytene chromosome map respectively, have resulted to the linkage of the wild type allele of
506 the *wp* and *tsl* genes to the male determining region of the Y chromosome. Thus, VIENNA 7
507 and VIENNA 8 males are heterozygous in the *wp* and *tsl* loci but phenotypically wild type while
508 VIENNA 7 and VIENNA 8 females are homozygous for the mutant alleles and phenotypically
509 white pupae and they die when exposed at elevated temperatures. The VIENNA 7 and
510 VIENNA 8 GSS can be constructed with and without the D53 inversion (VIENNA 7/8 $^{D53+}$ or $^{D53-}$
511). When the GSS have the inversion, females are homozygous ($^{D53+|+}$) for D53 while males are
512 heterozygous ($^{D53+|-}$) (6, 8, 16).
513
514 *Whole genome sequencing of* C. capitata *strains*
515 High-molecular-weight (HMW) DNA was extracted from *C. capitata* lines (males and females
516 of the wild type EgII strain, the VIENNA 7 $^{D53-|-}$ and VIENNA 8 $^{D53-|-}$ GSS and the inversion line
517 D53) and sequenced. Freshly emerged, virgin and unfed males and females were collected
518 from all strains. For 10X Genomics linked read and Nanopore sequencing, the HMW was
519 prepared as follows: twenty individuals of each sex and strain were pooled, ground in liquid
520 nitrogen, and HMW DNA was extracted using the QIAGEN Genomic tip 100/G kit (Qiagen,
521 Germany). For PacBio Sequel an EgII line was created with single pair crossing and
522 subsequent sibling-mating for six generations. In all generations adult and larval diet contained
523 100 µg/ml tetracycline. HMW DNA from G_6 individuals was prepared as follows: five males
524 from this EgII line were pooled and ground in liquid nitrogen, and HMW DNA was extracted
525 using the phenol/chloroform Phase Lock Gel™ tubes (QuantaBio) (53). DNA for Illumina
526 applications was extracted from individual flies (Table S1).
527 PacBio *de novo* sequencing: samples were purified with AMPure beads (Beckman Coulter,
528 UK) (0.6 volumes) and QC checked for concentration, size, integrity and purity using Qubit
529 (Qiagen, UK), Fragment Analyser (Agilent Technologies) and Nanodrop (Thermo Fisher)
530 machines. The samples were then processed without shearing using the PacBio Express kit
531 1 for library construction and an input of 4 µg DNA following the manufacturer's protocol. The
532 final library was size-selected using the Sage Blue Pippin (Sage Sciences) 0.75% cassette U1
533 marker in the range of 25-80 kb. The final library size and concentrations were obtained on
534 the Fragment Analyser before being sequenced using the Sequel 1 2.1 chemistry with V4
535 primers at a loading on plate concentration of 6 pM and 10 h movie times.
536 For Nanopore sequencing, the ligation sequencing kits SQK-LSK109 or SQK-RAD004
537 were used as recommended by the manufacturer (Oxford Nanopore Technologies, Oxford,
538 United Kingdom). Starting material for the ligation library preparation were 1 - 1.5 µg HMW
539 gDNA for the ligation libraries and 400 ng for the rapid libraries. The prepared libraries were

540 loaded onto FLO-PRO002 (R9.4) flow cells. Data collection was carried out using a
541 PromethION Beta with live high accuracy base calling for up to 72 h and with mux scan
542 intervals of 1.5 h. Each sample was sequenced at least twice. Data generated were 7.7 Gb
543 for EgII male, 31.09 Gb for D53 male, 26.72 Gb for VIENNA $7^{D53-|-}$ male, and 24.83 Gb for
544 VIENNA 8 $^{D53-|-}$ male. Run metrics are shown in Supplementary Table S5.
545 The PacBio data were assembled using CANU (54) with two parameter settings: the first
546 to avoid haplotype collapsing (genomeSize=500m corOutCoverage=200 "batOptions=-dg 3 -
547 db 3 -dr 1 -ca 500 -cp 50") and the second to merge haplotypes together (genomeSize=500m
548 corOutCoverage=200 correctedErrorRate=0.15). The genome completeness was assessed
549 with BUSCO v3 (44, 45) using the dipteran gene set (44). The two assemblies were found to
550 be "duplicated" due to alternative haplotypes. To improve the contiguity and reduce duplication
551 haploMerger2 was used (55). The new assembly was then retested with BUSCO v3 and used
552 scaffolding. Phase Genomics™ Hi-C libraries were made by Phase genomics from males
553 (n=2) of the same family used for PacBio sequencing. Initial scaffolding was completed by
554 Phase Genomics, but edited using the Salsa (56) and 3D-DNA
555 (https://github.com/theaidenlab/3d-dna) software. The resulting scaffolds were allocated a
556 chromosome number using chromosome specific marker described previously (16). Specific
557 attention was made to the assembly and scaffolding of chromosome 5. Two contig
558 misassemblies were detected by the Hi-C data and fitted manually. The new assembly
559 (EgII_Ccap3.2.1) was then validated using the Hi-C data. Genes were called using the
560 Funannotate software making use of the Illumina RNAseq data generated by this project;
561 mRNA mapping to the genome is described below.
562
563 *D53 breakpoint analysis in* C. capitata
564 To identify possible breakpoint positions, the Nanopore D53 fly assembly contig_531 was
565 mapped onto the EgII_scaffold_5 (from the EgII_CCAP3.2_CANU_Hi-C_scaffolds.fasta
566 assembly) using MashMap v2.0 (https://github.com/marbl/MashMap). This helped to visualize
567 the local alignment boundaries (Fig. S9A). MashMap parameters were set to kmer size = 16;
568 window size = 100; segment length = 500; alphabet = DNA; percentage identity threshold =
569 95%; filter mode = one-to-one.
570 Subsequent to this, and to help confirm the exact location of the identified breakpoints,
571 minimap2 (v2.17, https://github.com/lh3/minimap2) was used to align D53 as well as VIENNA
572 $8^{D53-|-}$ and VIENNA $7^{D53-|-}$ Nanopore reads onto the EgII scaffold_5 reference (Fig. S9B-C).
573 Minimap2 parameters for Nanopore reads were: minimap2 -x map-ont -A 1 -a --MD -L -t 40.
574 Samtools (v1.9, https://github.com/samtools/samtools) was used to convert the
575 alignment.sam to .bam and prepare the alignment file to be viewed in the Integrative Genomics
576 Viewer (IGV, http://software.broadinstitute.org/software/igv/). The expectation was to see a

577 leftmost breakpoint in D53 read set alignments but not in VIENNA 8$^{D53-|-}$ and VIENNA 7$^{D53-|-}$
578 when compared to the EgII reference (Fig.S9B). Due to an assembly gap in the EgII scaffold_5
579 sequence, the exact location of the leftmost inversion breakpoint was not conclusive using this
580 approach.
581 A complementary approach was then used to facilitate detection of the leftmost inversion
582 breakpoint in the D53 inversion line. Minimap2 was again used, but here D53 contig_531 was
583 used as reference for the mapping of EgII male PacBio reads as well as VIENNA $^{8D53-|-}$ male
584 and VIENNA 7 D53-|- male Nanopore reads (Fig. S10). Minimap2 parameters for PacBio
585 reads were: minimap2 -x map-pb -A 1 -a --MD -L -t 40. Minimap2 parameters for Nanopore
586 reads were: minimap2 -x map-ont -A 1 -a --MD -L -t 40. Samtools (v1.9,
587 https://github.com/samtools/samtools) was used to convert the alignment .sam to .bam and
588 prepare the alignment file to be viewed in the Integrative Genomics Viewer (IGV,
589 http://software.broadinstitute.org/software/igv/). The expectation was to see a common
590 breakpoint for all three of the above read set alignments when compared to the D53 genome
591 in the area of the inversion. Position ~3,055,294 was identified in the D53 contig_531 as the
592 most likely leftmost breakpoint.
593 To determine the rightmost breakpoint, D53 male and VIENNA 8 $^{D53-|-}$ and VIENNA 7$^{D53-|-}$
594 male nanopore reads were aligned on the EgII_scaffold_5 sequence. The expectation was to
595 see a breakpoint in D53 read set alignments but not in VIENNA 7$^{D53-|-}$ and VIENNA 8 $^{D53-|-}$. This
596 is the case here, since read alignments coming from both sides of the inversion are truncated
597 at one position (Fig. S9C). Findings from genome version EgII_Ccap3.2 were extrapolated to
598 the manually revised genome version EgII_Ccap3.2.1.
599 Predicted D53 inversion breakpoints were verified via PCRs in EgII, D53, and VIENNA 7^{D53+}
600 GSS male and female flies, using PhusionFlash Polymerase in a 10 µl reaction volume [98°C,
601 10 s; 30 cycles of (98°C, 1 s; 56°C, 5 s; 72°C, 35 s); 72°C, 1 min] (Fig. S4). The primer pair
602 for the right breakpoint was designed based on EgII sequence information, primers for the left
603 breakpoint were designed based on D53 sequence information. The wild type status of
604 chromosome 5 (EgII male and female, VIENNA 7 $^{D53+|-}$ male) was amplified using primer pairs
605 P_1794 and P_1798 (1,950 bp) and P_1795 and P_1777 (690 bp) (Table S4). Chromosome
606 5 with the inversion (D53 male and female, VIENNA 7 $^{D53+|-}$ male and VIENNA 7 $^{D53+|+}$ female)
607 was verified using primer pairs P_1777 and P_1798 (1,188 bp) and P_1794 and P_1795
608 (1,152 bp) and amplicon sequencing.
609
610 *RNA extraction for transcriptomic analysis of* C. capitata, B. dorsalis *and* Z. cucurbitae
611 Samples of *C. capitata*, *B. dorsalis* and *Z. cucurbitae* species were collected for RNA
612 extraction (Table S1) at 3rd instar larval and pre-pupal stages. Total RNA was extracted by
613 homogenizing three larvae of *C. capitata* and *B. dorsalis* and a single larvae of *Z. cucurbirtae*

614 in liquid nitrogen, and then using the RNeasy Mini kit (Qiagen). Three replicates per strain and
615 time point were performed. mRNA was isolated using the NEBNext polyA selection and the
616 Ultra II directional RNA library preparation protocols from NEB and sequenced on the Illumina
617 NovaSeq 6000 using duel indexes as 150 bp paired end reads (library insert 500 bp).
618 Individual libraries were sequenced to provide >1 million paired end reads per sample. Each
619 replicate was then assembled separately using Trinity (57). The assembled transcripts from
620 Trinity were mapped to the Ccap3.2 genome using minimap (58) (parameters -ax splice:hq -
621 uf). The Illumina reads were mapped with STAR (59). IGV v 2.6 (60) was used to view all data
622 at a genomic and gene level. Given that the white pupae GSS (12, 61) was used to collect
623 samples for RNA extraction from single larvae of *Z. cucurbitae*, larval sex was confirmed by a
624 maleness-specific PCR on the *MoY* gene of *Z. cucurbitae* (36) using cDNA synthesized with
625 the OneStep RT-PCR Kit (Qiagen) and the primer pair ZcMoY1F and ZcMoY1R (Table S4)
626 amplifying a 214 bp fragment. Conditions for a 25 µl PCR reaction using the 1× *Taq* PCR
627 Master Mix kit (Qiagen) were: [95°C, 5 min; 30 cycles of (95°C, 1 min; 51°C, 1 min; 72°C, 1
628 min); 72°C, 10 min]. Presence of a PCR product indicated a male sample. Each, male and
629 female sample was a pool of three individuals. Three replicates per strain and time point were
630 collected.
631
632 **Functional and cytogenetic verification of medfly D53 inversion and tephritid *wp* genes.**
633 Polytene chromosomes for *in situ* hybridization were prepared from third-instar larvae salivary
634 glands as described previously (62). In brief, the glands were dissected in 45% acetic acid
635 and placed on a coverslip in a drop of 3:2:1 solution (3 parts glacial acetic acid: 2 parts water:
636 1-part lactic acid) until been transparent (approximately 5 min). The coverslip was picked up
637 with a clean slide. After squashing, the quality of the preparation was checked by phase
638 contrast microscope. Satisfactory preparations were left to flatten overnight at -20°C and
639 dipped into liquid nitrogen until the babbling stopped. The coverslip was immediately removed
640 with razor blade and the slides were dehydrated in absolute ethanol, air dried and kept at room
641 temperature.
642 Probes were prepared by PCR. Single adult flies were used to extract DNA with the Extract
643 me kit (Blirt SA), following the manufacturer's protocol. NanoDrop spectrometer was used to
644 assess the quantity and quality of the extracted DNA which was then stored at -20°C until
645 used. Primers (P1790/1791, P1821/1822, Pgd_probe_F/R, vg1_probe_F/R, Sxl_probe_F/R,
646 y_probe_F/R, zw_probe_F/R, P1633/1634, Zc_F/R, Bd_F/R, P1395/1396, P1415/1416;
647 Table S4) were designed for each targeted gene using Primer 3 and/or Geneious Prime
648 programs. PCR was performed in a 25 µl reaction volume using 12.5 µl PCR Master mix 2x
649 Kit (Thermo Fisher Scientific), 60-80 ng DNA, and the following PCR settings [94°C, 5 min; 35
650 cycles of (94°C, 45 s; 56°C, 30 s; 72°C, 90 s); 72°C, 1 min].

651 The labelling of the probes was carried out according to the instruction manual of the Dig
652 DNA labelling kit (Roche). *In situ* hybridization was performed as described previously (63). In
653 brief, before hybridization, stored chromosome preparations were hydrated by placing them
654 for 2 min at each of the following ethanol solutions: 70%, 50% and 30%. Then they were
655 placed in 2× SSC at room temperature for 2 min. The stabilization of the chromosomes was
656 done by placing them in 2× SSC at 65°C for 30 min, denaturing in 0.07 M NaOH 2 min, washing
657 in 2× SSC for 30 sec, dehydrating (2 min in 30%, 50%, 70% and 95% ethanol), and air drying.
658 Hybridization was performed on the same day by adding 15 µl of denatured probe (boiled for
659 10 min and ice-chilled). Slides were covered with a siliconized coverslip, sealed with rubber
660 cement, and incubated at 45°C overnight in a humid box. At the end of incubation, the
661 coverslip was floated off in 2x SSC and the slide washed in 2x SSC for 3 x 20 min at 53°C.
662 After 5 min wash in Buffer 1 (100 mM tris-HCl pH 7.5/ 1.5 M NaCl), the preparations were
663 in Blocking solution (Blocking reagent 0.5% in Buffer 1) for 30 min, and then washed for 1 min
664 in Buffer 1. The antibody mix was added to each slide and a coverslip was added. Then the
665 slides were incubated in a humid box for 45 min at room temperature, following 2× 15 min
666 washes in Buffer 1, and a 2 min wash in detection buffer (100 mM Tris-HCl pH 9.5/ 100 mM
667 NaCl). The color was developed with 1 ml of NBT/BCIP solution during a 40 min incubation in
668 the dark at room temperature. The removal of the NBT/BCIP solution was done by rinsing in
669 water twice. Hybridization sites were identified and photographed using a 40× objective or
670 100× oil objectives (phase or bright field), with reference to the salivary gland chromosome
671 maps (64).
672
673 **Gene editing and generation of homozygous *wp*$^{-}$ strains in *B. tryoni* and *C. capitata*.** For
674 CRISPR/Cas9 gene editing in *B. tryoni*, purified Cas9 protein (Alt-R® S.p. Cas9 Nuclease V3,
675 #1081058, 10 µg/µl) and guide RNAs (customized Alt-R® CRISPR/Cas9 crRNA, 2 nmol and
676 Alt-R® CRISPR/Cas9 tracrRNA, #1072532, 5nmol) were obtained from Integrated DNA
677 Technologies (IDT) and stored at -20°C. The guide RNAs were individually resuspended to a
678 100 µM stock solution with nuclease-free duplex buffer and stored at -20°C before use. The
679 two customized 20 bp crRNA sequences (Bt_MFS-1 and Bt_MFS-2) (Table S4) were
680 designed using CRISPOR (65). Injection mixes for microinjection of *B. tryoni* embryos
681 comprise of 300 ng/µl Cas9 protein, 59 ng/µl of each individual crRNA, 222 ng/µl tracrRNA
682 and 1x injection buffer (0.1 mM sodium phosphate buffer pH 6.8, 5 mM KCl) in a final volume
683 of 10 µl. The guide RNA complex containing the two crRNAs and tracrRNA was initially
684 prepared by heating the mix at 95°C for 5 min before cooling to room temperature. The Cas9
685 enzyme along with the rest of the injection mix components were then added to the guide RNA
686 complex and incubated at room temperature for 5 minutes to assemble the RNP complexes.
687 Microinjections were performed in *B. tryoni* Ourimbah laboratory strain embryos that were

688 collected over 1 hour time period and prepared for injection as previously described (22).
689 Injections were performed under paraffin oil using borosilicate capillary needles (#30-0038,
690 Harvard Apparatus) drawn out on a Sutter P-87 flaming/brown micropipette puller and
691 connected to an air-filled 20 ml syringe, a manual MM-3 micromanipulator (Narishige) and a
692 CKX31-inverted microscope (Olympus). Microscope slides with the injected embryos were
693 placed on agar in a Petri dish that was then placed in a vented container containing moist
694 paper towels at 25°C (± 2°C). Hatched first instar larvae were removed from the oil and
695 transferred to larval food. Individual G_0 flies were crossed to six virgin flies from the Ourimbah
696 laboratory strain and eggs were collected overnight for two consecutive weeks. G_1 flies were
697 then allowed to mate *inter se* and eggs were collected in the same manner. G_2 pupae were
698 then analyzed phenotypically and separated according to color of pupae (brown, mosaic or
699 white).
700 For *C. capitata* CRISPR/Cas9 gene editing, lyophilized Cas9 protein (PNA Bio Inc, CP01)
701 was reconstituted to a stock concentration of 1 µg/µl in 20 mM Hepes, 150 mM KCl, 2%
702 sucrose and 1 mM DTT (pH 7.5) and stored at -80°C until use. A guide RNA (gRNA_MFS),
703 targeting the third CDS exon of *CcMFS* was designed and tested for potential off target effects
704 using Geneious Prime (52) and the *C. capitata* genome annotation Ccap2.1. *In silico* target
705 site analysis predicted an on-target activity score of 0.615 (scores are between 0 and 1; the
706 higher the score the higher the expected activity (66) and zero off-targets sites in the medfly
707 genome. Guide RNA was synthesized by *in vitro* transcription of linear double-stranded DNA
708 template as previously described (67) using primers P_1753 and P_369 (Table S4), Q5 HF
709 polymerase, and a Bio-Rad C1000 Touch thermal cycler [98°C, 30 s; 35 cycles of (98°C, 10
710 s; 58°C, 20 s; 72°C, 20 s); 72°C, 2 min] and HiScribe™ T7 High Yield RNA Synthesis. Injection
711 mixes for microinjection of embryos contained 360 ng/µl Cas9 protein (1 µg/µl, dissolved in its
712 formulation buffer), 200 ng/µl gRNA_MFS and an end-concentration of 300 mM KCl according
713 to previous studies (67, 68). The mix was freshly prepared on ice followed by an incubation
714 step for 10 min at 37°C to allow pre-assembly of gRNA-Cas9 ribonucleoprotein complexes
715 and stored on ice prior to injections. Microinjections were conducted in wild type EgII *C.*
716 *capitata* embryos. Eggs were collected over a 30-40 min time period and prepared for injection
717 as previously described (67). Injections were performed using siliconized quartz glass needles
718 (Q100-70-7.5; LOT171381; Science Products, Germany), drawn out on a Sutter P-2000 laser-
719 based micropipette puller. The injection station consisted of a manual micromanipulator (MN-
720 151, Narishige), an Eppendorf FemtoJet 4i microinjector, and an Olympus SZX2-TTR
721 microscope (SDF PLAPO 1xPF objective). The microscope slide with the injected embryos
722 was placed in a Petri dish containing moist tissue paper in an oxygen chamber (max. 2 psi).
723 Hatched first instar larvae were transferred from the oil to larval food.

724 As complementation assay, reciprocal crosses between surviving G_0 adults and virgin *white*
725 *pupae* strain #1402_22m1B (pBac_*fa_attP-TREhs43-Cctra-I-hid*^{Ala5}*-SV40_a_PUb-nls-EGFP-*
726 *SV40*) (*wp*$^{-(nat)}$) (24) were set up either single paired (six cages) or in groups of seven to ten
727 flies (seven cages). Eggs were collected three times every 1-2 days. Progeny (G_1) exhibiting
728 the *white pupae* phenotype (*wp*$^{-(nat)|-(CRISPR)}$) were assayed via non-lethal genotyping and
729 sorted according to mutation genotype (see Fig. 4). Genotypes 'A-H' were group-backcrossed
730 into WT EgII (*wp*$^{+|+}$), genotype 'C' siblings massed crossed. Eggs were collected 4 times every
731 1-2 days. Generation G_2 flies were analyzed via PCR using three primers, specific for *wp*$^{+}$ and
732 *wp*$^{-(CRISPR)}$ or *wp*$^{-(nat)}$ allele size respectively. Offspring of outcross cages showed brown pupae
733 phenotype and either *wp*$^{+|-(nat)}$ or *wp*$^{+|-(CRISPR)}$ genotype. In order to make mutations A, D, and
734 H homozygous, 40 flies (25 females, 15 males) were genotyped each, and *wp*$^{+|-(CRISPR)}$ positive
735 flies were inbred (mutation A: 15 females, 7 males, mutation D: 12 females, 7 males, mutation
736 H: 11 females, 8 males). G_3 showing white pupae phenotype was homozygous for *wp*$^{-(CRISPR)}$
737 mutations A, D, or H, respectively and was used to establish lines. Inbreeding of mutation C
738 *wp*$^{-(nat)|-(CRISPR)}$ flies produced only white pupae offspring, based on either *wp*$^{-(nat)|-(nat)}$, *wp*$^{-(nat)|-}$
739 $^{(CRISPR)}$ or *wp*$^{-(CRISPR)|-(CRISPR)}$. 94 flies (46 females, 48 males) were genotyped, homozygous *wp*$^{-}$
740 $^{(CRISPR)}$ were inbred to establish a line (13 females, 8 males).
741
742 **Molecular analyses of *wp* mutants and mosaics.** In *B. tryoni,* genomic DNA was isolated
743 for genotyping from G_2 pupae using the DNeasy Blood and Tissue Kit (Qiagen). PCR
744 amplicons spanning both BtMFS guide recognition sites were generated using Q5 polymerase
745 (NEB) with primers BtMFS_5primeF and BtMFS_exon2R (Table S4). Products were purified
746 using MinElute PCR Purification Kit (Qiagen), ligated into pGEM-t-easy vector (Promega) and
747 transformed into DH5α cells. Plasmids were purified with Wizard *Plus* SV Minipreps
748 (Promega) and sequenced.
749 In *C. capitata,* non-lethal genotyping was performed to identify parental genotypes before
750 setting up crosses. Therefore, genomic DNA was extracted from single legs of G_1 and G_2 flies
751 following a protocol established by Carvalho et al. (69). Single legs of anesthetized flies were
752 cut at the proximal femur using scissors. Legs were then homogenized by ceramic beads and
753 50 µl buffer (10 mM Tris-Cl, pH 8.2, 1 mM EDTA, 25 mM NaCl) for 15 s (6 m/s) using a
754 FastPrep-24™ 5G homogenizer. Then, 30 µl buffer and 1.7 µl proteinase-K (2.5 U/mg) were
755 added, incubated for 1 h at 37°C and the reaction stopped by 4 min at 98°C. The reaction mix
756 was cooled down on ice and used for PCR. For G_1 flies, PCR on *wp* was performed in a 25 µl
757 reaction volume using the Dream*Taq* polymerase, primer pair P_1643 and P_1644 (Table
758 S4), and 3.75 µl reaction mix. Different amplicon sizes are expected for brown (*wp*$^{+}$ and
759 *wp*$^{-(CRISPR)}$) and white pupae (*wp*$^{-(nat)}$) alleles, 724 bp and 8,872 bp in size, respectively. The
760 *wp*$^{-(nat)}$ amplicon was excluded via PCR settings [95°C, 3 min; 35 cycles of (95°C, 30 s; 56°C,

761 30 s; 72°C, 1 min); 72°C, 5 min]. The 724 bp PCR product was verified by agarose
762 electrophoresis and purified from the PCR reaction using the DNA Clean & Concentrator™-5
763 kit. PCR products were sequenced using primer P_1644 and sequences analyzed using the
764 Geneious Prime Software Package (6). In generation G_2, flies were analyzed using multiplex
765 PCR with primers P_1657, P_1643, and P_1644 (Table S4), to distinguish between the *wp*$^{-(nat)}$
766 (457 bp; P_1643 and P_1657), and *wp*$^{-(CRISPR)}$ alleles (724 bp; P_1643 and P1644) using
767 the PCR protocol [95°C, 3 min; 35 cycles of (95°C, 30 s; 56°C, 30 s; 72°C, 1 min); 72°C, 5
768 min]).
769
770 **Image acquisition.** Images of *B. tryoni* pupae were taken with an Olympus SZXI6
771 microscope, Olympus DP74 camera and Olympus LF-PS2 light source using the Olympus
772 stream basic 2.3.3 software. Images of *C. capitata* pupae were taken with a Keyence digital
773 microscope VHX-5000. Image processing was conducted with Adobe Photoshop CS5.1
774 software to apply moderate changes to image brightness and contrast. Changes were applied
775 equally across the entire image and throughout all images.

Ethics approval and consent to participate

Not applicable

Consent for publication

Not applicable

Availability of data and material

All data generated or analyzed are included in this article.

Declaration of interest

none

Funding

This study was financially supported by the Joint FAO/IAEA Insect Pest Control Subprogramme of the Joint FAO/IAEA Division of Nuclear Techniques in Food and Agriculture. The project has also been funded by the Horticulture Innovation Australia (FF17000, FF18002), using funds from the Australian Government, and co-investment from Macquarie University and South Australian Research and Development Institute (SARDI). SWB was supported by the Australian Research Council (FT140101303) and Hermon Slade Foundation grant HSF 18/6. Furthermore, this work was supported by the Emmy Noether program of the German Research Foundation (SCHE 1833/1-1; to MFS) and the LOEWE Center for Insect Biotechnology and Bioresources of the Hessen State Ministry for Higher Education, Research and the Arts (HMWK; to MFS). The work was also supported by Canadian Foundation for Innovation and Genome Canada Genome Technology Platform awards and the International Atomic Energy Agency research contact no. 23358 as part of the Coordinated Research Project “Generic approach for the development of genetic sexing strains for SIT applications” (JR).

Acknowledgements

This study was benefitted from discussions at International Atomic Energy Agency funded meetings for the Coordinated Research Projects (CRPs) and particularly the CRP on “Generic approach for the development of genetic sexing strains for SIT applications”. The authors also wish to thank Tanja Rehling, Jakob Martin and Johanna Rühl for technical assistance and Germano Sollazzo for helping with injections and primers design (Justus-Liebig University Gießen and Insect Pest Control Laboratory); Elena Isabel Cancio Martinez, Thilakasiri Dammalage, Sohel Ahmad and Gülizar Pillwax for insect rearing (Insect Pest Control Laboratory), Shu-Huang Chen (McGill University) for technical assistance with Nanopore library preparations; and Arjen van´t Hof (University of Liverpool) for constructing libraries from micro-dissected chromosomes for Illumina sequencing.

References

1. A. S. Robinson, G. Hooper, *Fruit flies: their biology, natural enemies, and control* (Elsevier, Amsterdam; New York, 1989), vol. 1, pp. 372.
2. D. M. Suckling *et al.*, Eradication of tephritid fruit fly pest populations: outcomes and prospects. *Pest Manag Sci* **72**, 456-465 (2016).
3. V. A. Dyck *et al.*, "Management of area-wide integrated pest management programmes that integrate the sterile insect technique" in *Sterile insect technique - principles and practice in area-wide integrated pest management,* V. A. Dyck, J. Hendrichs, A. S. Robinson, Eds. (Springer, Dordrecht, NL, 2005), pp. 525-545.
4. M. Vreysen, A. S. Robinson, J. Hendrichs, *Area-wide control of insect pests: from research to field implementation*. M. Vreysen, A. S. Robinson, J. Hendrichs, Eds. (Springer, Dordrecht, NL, 2007).
5. P. Rendon, D. McInnis, D. Lance, J. Stewart, Medfly (Diptera: Tephritidae) genetic sexing: large-scale field comparison of males-only and bisexual sterile fly releases in Guatemala. *Journal of Economic Entomology* **97**, 1547-1553 (2004).
6. G. Franz, "Genetic sexing strains in Mediterranean fruit fly, an example for other species amenable to large-scale rearing for the sterile insect technique" in *Sterile insect technique - principles and practice in area-wide integrated pest management,* V. A. Dyck, J. Hendrichs, A. S. Robinson, Eds. (Springer, Dordrecht, NL, 2005), pp. 427-451.
7. A. A. Augustinos *et al.*, *Ceratitis capitata* genetic sexing strains: laboratory evaluation of strains from mass-rearing facilities worldwide. *Entomologia Experimentalis et Applicata* **164**, 305-317 (2017).
8. A. Zacharopoulou *et al.*, A review of more than 30 years of cytogenetic studies of Tephritidae in support of sterile insect technique and global trade. *Entomologia Experimentalis et Applicata* **164**, 204-225 (2017).
9. Y. Rössler, The genetics of the Mediterranean fruit fly: a “white pupae” Mutant. *Annals of the Entomological Society of America* **72**, 583-585 (1979).
10. Y. Rössler, Y. Koltin, The genetics of the Mediterranean fruit fly, *Ceratitis capitata*: three morphological mutations. *Annals of the Entomological Society of America* **69**, 604-608 (1976).
11. S. D. McCombs, S. H. Saul, Linkage analysis of five new genetic markers of the oriental fruit fly, *Bactrocera dorsalis* (Diptera: Tephritidae). *The Journal of heredity* **83**, 199-203 (1992).
12. D. O. McInnis *et al.*, Development of a pupal color-based genetic sexing strain of the melon fly, *Bactrocera cucurbitae* (Coquillett) (Diptera: Tephritidae). *Annals of the Entomological Society of America* **97**, 1026-1033 (2004).
13. P. Wappner *et al.*, *White pupa: A Ceratitis capitata mutant lacking catecholamines for tanning the puparium* (1995), vol. 25, pp. 365-373.
14. Y. Rössler, H. Rosenthal, Genetics of the Mediterranean fruit fly (Diptera: Tephritidae): morphological mutants on chromosome five. *Annals of the Entomological Society of America* **85**, 525-531 (1992).
15. P. Kerremans, G. Franz, Cytogenetic analysis of chromosome 5 from the Mediterranean fruit fly, *Ceratitis capitata*. *Chromosoma* **103**, 142-146 (1994).
16. A. Papanicolaou *et al.*, The whole genome sequence of the Mediterranean fruit fly, *Ceratitis capitata* (Wiedemann), reveals insights into the biology and adaptive evolution of a highly invasive pest species. *Genome Biology* **17**, 192 (2016).
17. P. A. Papathanos *et al.*, A perspective on the need and current status of efficient sex separation methods for mosquito genetic control. *Parasites & Vectors* **11**, 654 (2018).
18. S. B. Sim, S. M. Geib, A chromosome-scale assembly of the *Bactrocera cucurbitae* genome provides insight to the genetic basis of *white pupae*. *G3 (Bethesda, Md.)* **7**, 1927-1940 (2017).

19. S. B. Sim, R. Ruiz-Arce, N. B. Barr, S. M. Geib, A new diagnostic resource for *Ceratitis capitata* strain identification based on QTL mapping. *G3 (Bethesda, Md.)* **7**, 3637-3647 (2017).
20. E. M. Zdobnov *et al.*, OrthoDB v9.1: cataloging evolutionary and functional annotations for animal, fungal, plant, archaeal, bacterial and viral orthologs. *Nucleic Acids Res* **45**, D744-D749 (2017).
21. M. San Jose *et al.*, Incongruence between molecules and morphology: A seven-gene phylogeny of *Dacini* fruit flies paves the way for reclassification (Diptera: Tephritidae). *Mol Phylogenet Evol* **121**, 139-149 (2018).
22. A. Choo, P. Crisp, R. Saint, L. V. O'Keefe, S. W. Baxter, CRISPR/Cas9-mediated mutagenesis of the white gene in the tephritid pest *Bactrocera tryoni*. *Journal of Applied Entomology* **142**, 52-58 (2018).
23. A. Gariou-Papalexiou *et al.*, Polytene chromosomes as tools in the genetic analysis of the Mediterranean fruit fly, *Ceratitis capitata*. *Genetica* **116**, 59-71 (2002).
24. C. E. Ogaugwu, M. F. Schetelig, E. A. Wimmer, Transgenic sexing system for *Ceratitis capitata* (Diptera: Tephritidae) based on female-specific embryonic lethality. *Insect Biochemistry and Molecular Biology* **43**, 1-8 (2013).
25. A. W. Davis *et al.*, Rescue of hybrid sterility in crosses between *D. melanogaster* and *D. simulans*. *Nature* **380**, 157-159 (1996).
26. L. O. Araripe, H. Montenegro, B. Lemos, D. L. Hartl, Fine-scale genetic mapping of a hybrid sterility factor between *Drosophila simulans* and *D. mauritiana*: the varied and elusive functions of "speciation genes". *BMC Evol Biol* **10**, 385 (2010).
27. N. J. Brideau, D. A. Barbash, Functional conservation of the Drosophila hybrid incompatibility gene Lhr. *BMC Evol Biol* **11**, 57 (2011).
28. A. A. Kotov *et al.*, piRNA silencing contributes to interspecies hybrid sterility and reproductive isolation in *Drosophila melanogaster*. *Nucleic Acids Res* **47**, 4255-4271 (2019).
29. D. A. Barbash, Ninety years of *Drosophila melanogaster* hybrids. *Genetics* **186**, 1-8 (2010).
30. D. G. Bedo, A. Zacharopoulou, Inter-tissue variability of polytene chromosome banding patterns. *Trends Genet* **4**, 90-91 (1988).
31. E. V. Kriventseva *et al.*, OrthoDB v10: sampling the diversity of animal, plant, fungal, protist, bacterial and viral genomes for evolutionary and functional annotations of orthologs. *Nucleic Acids Res* **47**, D807-d811 (2019).
32. Y. Zhao *et al.*, A major facilitator superfamily protein participates in the reddish brown pigmentation in *Bombyx mori*. *J Insect Physiol* **58**, 1397-1405 (2012).
33. The modEncode Consortium *et al.*, Identification of functional elements and regulatory circuits by Drosophila modENCODE. *Science (New York, N.Y.)* **330**, 1787-1797 (2010).
34. T. R. Wright, The genetics of biogenic amine metabolism, sclerotization, and melanization in *Drosophila melanogaster*. *Adv Genet* **24**, 127-222 (1987).
35. K. Bourtzis, C. Psachoulia, V. J. Marmaras, Evidence that different integumental phosphatases exist during development in the Mediterranean fruit fly *Ceratitis capitata*: possible involvement in pupariation. *Comparative Biochemistry and Physiology Part B: Comparative Biochemistry* **98**, 411-416 (1991).
36. A. Meccariello *et al.*, *Maleness-on-the-Y* (*MoY*) orchestrates male sex determination in major agricultural fruit fly pests. *Science* **365**, 1457-1460 (2019).
37. A. B. Hall *et al.*, Sex determination. A male-determining factor in the mosquito *Aedes aegypti*. *Science* **348**, 1268-1270 (2015).
38. P. Liu *et al.*, *Nix* is a male-determining factor in the Asian tiger mosquito *Aedes albopictus*. *Insect Biochem Mol Biol* **118**, 103311 (2019).
39. C. M. Ward, T. H. To, S. M. Pederson, ngsReports: a Bioconductor package for managing FastQC reports and other NGS related log files. *Bioinformatics* **36**, 2587-2588 (2020).

40. F. J. Sedlazeck, P. Rescheneder, A. von Haeseler, NextGenMap: fast and accurate read mapping in highly polymorphic genomes. *Bioinformatics* **29**, 2790-2791 (2013).
41. E. Garrison, G. Marth, Haplotype-based variant detection from short-read sequencing. arXiv:1207.3907.
42. H. Li, A statistical framework for SNP calling, mutation discovery, association mapping and population genetical parameter estimation from sequencing data. *Bioinformatics* **27**, 2987-2993 (2011).
43. X. Zheng *et al.*, SeqArray-a storage-efficient high-performance data format for WGS variant calls. *Bioinformatics* **33**, 2251-2257 (2017).
44. F. A. Simão, R. M. Waterhouse, P. Ioannidis, E. V. Kriventseva, E. M. Zdobnov, BUSCO: assessing genome assembly and annotation completeness with single-copy orthologs. *Bioinformatics* **31**, 3210-3212 (2015).
45. R. M. Waterhouse *et al.*, BUSCO applications from quality assessments to gene prediction and phylogenomics. *Mol Biol Evol* **35**, 543-548 (2018).
46. A. Stamatakis, RAxML version 8: a tool for phylogenetic analysis and post-analysis of large phylogenies. *Bioinformatics* **30**, 1312-1313 (2014).
47. C. Zhang, M. Rabiee, E. Sayyari, S. Mirarab, ASTRAL-III: polynomial time species tree reconstruction from partially resolved gene trees. *BMC Bioinformatics* **19**, 153 (2018).
48. S. H. Martin, S. M. Van Belleghem, Exploring evolutionary relationships across the genome using topology weighting. *Genetics* **206**, 429-438 (2017).
49. R. D. Finn, J. Clements, S. R. Eddy, HMMER web server: interactive sequence similarity searching. *Nucleic Acids Res* **39**, W29-37 (2011).
50. H. Li *et al.*, The Sequence Alignment/Map format and SAMtools. *Bioinformatics* **25**, 2078-2079 (2009).
51. A. V. Zimin *et al.*, The MaSuRCA genome assembler. *Bioinformatics* **29**, 2669-2677 (2013).
52. M. Kearse *et al.*, Geneious Basic: an integrated and extendable desktop software platform for the organization and analysis of sequence data. *Bioinformatics* **28**, 1647-1649 (2012).
53. M. R. Green, J. Sambrook, Isolation of High-Molecular-Weight DNA using organic solvents. *Cold Spring Harb Protoc* **2017**, pdb.prot093450 (2017).
54. S. Koren *et al.*, Canu: scalable and accurate long-read assembly via adaptive k-mer weighting and repeat separation. *Genome Res* **27**, 722-736 (2017).
55. S. Huang *et al.*, HaploMerger: reconstructing allelic relationships for polymorphic diploid genome assemblies. *Genome Res* **22**, 1581-1588 (2012).
56. J. Ghurye, M. Pop, S. Koren, D. Bickhart, C. S. Chin, Scaffolding of long read assemblies using long range contact information. *BMC Genomics* **18**, 527 (2017).
57. B. J. Haas *et al.*, De novo transcript sequence reconstruction from RNA-seq using the Trinity platform for reference generation and analysis. *Nat Protoc* **8**, 1494-1512 (2013).
58. H. Li, Minimap2: pairwise alignment for nucleotide sequences. *Bioinformatics* **34**, 3094-3100 (2018).
59. A. Dobin *et al.*, STAR: ultrafast universal RNA-seq aligner. *Bioinformatics* **29**, 15-21 (2013).
60. J. T. Robinson *et al.*, Integrative genomics viewer. *Nature biotechnology* **29**, 24-26 (2011).
61. A. Zacharopoulou, G. Franz, Genetic and cytogenetic characterization of genetic sexing strains of *Bactrocera dorsalis* and *Bactrocera cucurbitae* (Diptera: Tephritidae). *J Econ Entomol* **106**, 995-1003 (2013).
62. A. Zacharopoulou *et al.*, The genome of the Mediterranean fruit fly *Ceratitis capitata*: localization of molecular markers by *in situ* hybridization to salivary gland polytene chromosomes. *Chromosoma* **101**, 448-455 (1992).
63. P. Mavragani-Tsipidou *et al.*, "Protocols for cytogenetic mapping of arthropod genomes: Tephritid fruit flies of economic importance" in *Protocols for cytogenetic*

971 *mapping of arthropod genomes,* I. Sakharov, Ed. (CRC Press, Taylor and Francis
972 Group, LLC, Florida, USA 2014), pp. 1-62.
973 64. A. Zacharopoulou, Polytene chromosome maps in the medfly *Ceratitis capitata*
974 *Genome* **33**, 184–197 (1990).
975 65. J. P. Concordet, M. Haeussler, CRISPOR: intuitive guide selection for CRISPR/Cas9
976 genome editing experiments and screens. *Nucleic Acids Res* **46**, W242-W245
977 (2018).
978 66. J. G. Doench *et al.*, Rational design of highly active sgRNAs for CRISPR-Cas9-
979 mediated gene inactivation. *Nature biotechnology* **32**, 1262-1267 (2014).
980 67. R. A. Aumann, M. F. Schetelig, I. Häcker, Highly efficient genome editing by
981 homology-directed repair using Cas9 protein in *Ceratitis capitata*. *Insect Biochemistry*
982 *and Molecular Biology* **101**, 85-93 (2018).
983 68. A. Burger *et al.*, Maximizing mutagenesis with solubilized CRISPR-Cas9
984 ribonucleoprotein complexes. *Development (Cambridge, England)* **143**, 2025-2037
985 (2016).
986 69. G. B. Carvalho, W. W. Ja, S. Benzer, Non-lethal PCR genotyping of single
987 Drosophila. *Biotechniques* **46**, 312-314 (2009).

988